

Characterization of Cementitious Materials Exposed to Freezing and Thawing in Combination with Deicing Salts Using 3D Scans

Alexander Haynack,* Jithender J. Timothy, Thomas Kränkel, and Christoph Gehlen

Surface deterioration of concrete subjected to freezing and thawing in combination with deicing salts is one of the most important factors determining the durability of concrete infrastructure in cold climates. The freeze–thaw deicing salt (FTDS) resistance of cementitious materials can be determined by the capillary suction of de-icing chemicals and freeze–thaw (CDF) test. Specimens are subjected to repeated freeze–thaw cycles with simultaneous addition of deicing salt and the amount of material scaled off near the surface is determined. For concretes with adequate FTDS resistance, this test method works very well. However, specimens with unknown performance often experience increased edge scaling. This leads to a falsification of results and consequently to an underestimation of the actual freeze–thaw resistance. In materials research, however, concretes with high levels of surface deterioration are studied in order to investigate various factors of influence on the freeze–thaw resistance of concretes in a targeted manner. This article presents a novel methodology that delivers new information regarding surface deterioration of CDF samples using high-resolution 3D scan data. Change of volume is used to support deterioration results of the standard CDF methodology. Increase of surface area is used to estimate change in roughness of samples.

1. Introduction

By 2050, 70% of the world's population is expected to live in urban areas.^[1] For this reason, huge investments in concrete infrastructure will be required. Improving the sustainability of concrete infrastructure is of utmost importance. Extending the

A. Haynack, J. J. Timothy, T. Kränkel, C. Gehlen
TUM School of Engineering and Design
Department of Materials Engineering, Chair of Materials Science and Testing
Centre for Building Materials (CBM)
Technical University of Munich
81245 Munich, BY, Germany
E-mail: alexander.haynack@tum.de

 The ORCID identification number(s) for the author(s) of this article can be found under <https://doi.org/10.1002/adem.202300265>.

© 2023 The Authors. Advanced Engineering Materials published by Wiley-VCH GmbH. This is an open access article under the terms of the Creative Commons Attribution-NonCommercial-NoDerivs License, which permits use and distribution in any medium, provided the original work is properly cited, the use is non-commercial and no modifications or adaptations are made.

DOI: 10.1002/adem.202300265

service life of concrete infrastructure is one of the most important components to improve sustainability. Freeze–thaw deicing salt (FTDS)-induced damage is a major effect on the durability of concrete in cold climates,^[2] e.g., damage to concrete pavements caused by freezing during winter. Such damages are mainly initiated by moisture transport into the concrete. Transport processes in concrete largely depend on the distribution, amount, type, size, and shape of the capillary pores within the system.^[3] The formation of these pores is caused by excess water, which is not used for the hydration process and therefore bound neither chemically nor physically. The resulting capillary pore structure enables the intrusion of gases and liquids into the concrete.^[4]

Deterioration induced by exposing the material to freezing and thawing loads can be categorized into scaling of the surface and internal microcracking. **Figure 1** shows the surface deterioration of a concrete wall with a high saturation freezing

and thawing exposure at a floodgate in Germany. The 10 year old building, composed of a blast furnace slag cement (CEM III/A according to DIN EN 197-1^[5]), shows several freeze–thaw-induced surface damages in the water splash zone.

Fundamental contributions to our current understanding of freeze–thaw-induced deterioration of cement-based materials include the work of Setzer (thermal equilibrium/micro-ice-lens model),^[6] Powers and Helmuth (osmotic pressure),^[7] Coussy and Monteiro (poromechanics),^[8] Scherer (crystallization pressure),^[9,10] Zhao (nanofluidic salt inclusions),^[11] and Timothy.^[12] These theories formed the basis for the development of a variety of analytical and computational models for model-based characterization of freeze–thaw-induced damage to cementitious materials. An accurate depiction of the deterioration process will potentially improve our current understanding of the deterioration mechanisms.

The CDF test (according to DIN CEN/TS 12 390-9:2017-05^[13]) is considered as the standard test method for determining the freeze–thaw resistance of concrete in Germany. Here, the concrete or mortar specimens are cyclically exposed to temperatures from 20 to –20 °C over the course of 12 h. This so-called freeze–thaw cycle (FTC) is repeated 28 times. The decisive test criterion



Figure 1. Surface deterioration of a concrete wall with a high saturation freezing and thawing exposure at a floodgate in Germany.



Figure 2. CDF sample showing the detachment of the isolation tape.

is the surface deterioration of the sample surface. For isolation purposes and a guaranteed 1D freeze–thaw exposition, the vertical planes of the specimens are sealed with aluminum laminated butyl rubber film.^[14] Concrete mixtures with high surface deterioration cause the isolation to scale off which results in a 2D exposition and an increased surface deterioration in the peripheral areas of the specimens (see **Figure 2**).

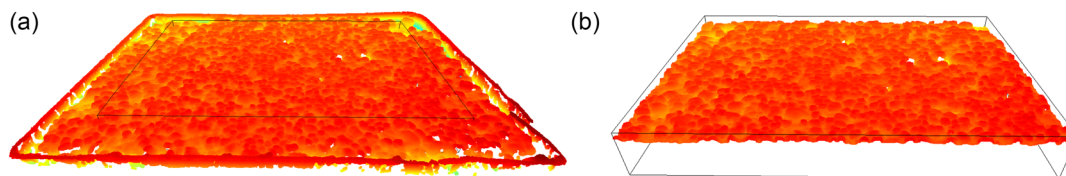


Figure 3. Scanned surfaces of a CDF specimen: a) original, scaled surface; b) sample surface after the removal of the peripheral areas. The black lines symbolize the area considered for subsequent evaluation.

The use of 3D scanning technology has already been proven in the field of mechanical engineering.^[15–18] It is mainly used for quality control and reverse engineering by comparing scan data with their respective digital models. As a result, the scan-to-model differences such as weld joints, deformations, and other deviations are detected and analyzed.^[18] The idea of this target–actual comparison is applied to the field of damage assessment of concrete after freeze–thaw- and deicing salt-induced expositions. For this, the test samples are scanned after certain FTC and afterward aligned to a reference scan before freeze–thaw exposition. This allows the detection of the surface deterioration and degradation caused by repeated FTC. Weise^[19] has used a similar approach with photogrammetry to characterize the height profile of concrete samples after increasing FTC. The problem of isolation tape scaling can also be countered with this novel methodology by simply removing the peripheral areas of the sample (see **Figure 3**) and therefore excluding it from the analysis.

The device used for this study is the HandySCAN Black Elite by Creaform.^[20] It shows an accuracy of 25 μm , which has been confirmed by calibration measurements prior to this study. The hand-held design of the device delivers a high performance and a great suitability for the presented application.

The main focus of this article lies on the description of the development of the 3D scan alignment algorithm and the consequent data analysis. The main goal of this research was to reduce the underestimation of the results of CDF samples caused by the detachment of the lateral isolation tape at high levels of surface deterioration.

2. Materials

The mix designs of mortars used in this study consist of an Ordinary Portland cement with strength class 42.5 N mm^{-2} (CEM I 42.5 N according to DIN EN 197-1^[5]) with a maximum aggregate size of either 2 mm (M1) or 0.5 mm (M2). Both mixtures had a w/c ratio of 0.55 and were held in the framework for 1 day. After the removal of the framework, the samples were stored under water until a sample age of 7 days. Subsequently, the mortar samples were stored in standard climate conditions of 20 °C and 65% relative humidity for 21 days until the sample age of 28 days according to ref. [14]. Additionally, another set of samples from mixture M1 has been stored completely under water before testing. One set of samples consists of five individual mortar samples with the dimensions of 15 × 11 × 7 cm^3 . The applied preconditioning and the composition of the sample sets used in this study are given in **Table 1**.

Table 1. Preconditioning and composition of mortar samples.

Label	Preconditioning	W/C	Cement [kg m ⁻³]	Water [kg m ⁻³]	Aggregates [kg m ⁻³]	Max. aggr. size [mm]
M1 20–65	20 °C, 65% RH	0.55	560	308	1312	2
M1 WS	Water storage	0.55	560	308	1312	2
M2 20-65	20 °C, 65% RH	0.55	730	401.5	932	0.5

3. Capillary Suction of Deicing Chemicals and Freeze–Thaw Test (CDF)

After reaching a sample age of 28 days, the samples were placed on 5 mm spacers inside of CDF containment boxes. The boxes were then filled with a 3% sodium chloride (NaCl) solution up to a height of 10 mm from the bottom of the containment box. Within the 7 day period of capillary resaturation, the NaCl solution can be absorbed by the samples. After that, the cyclical freeze–thaw exposition from 20 to –20 °C (see **Figure 4**) is started for a total duration of 14 days. This complies to 28 FTC. The magnitude of the measured temperature T_{measured} from embedded sensors in an equivalent specimen is consistent with the applied exposition temperatures T_{applied} . However, as shown in **Figure 4**, there is a slight temporal lag due to the material and ambient conditions surrounding the specimen.

Throughout the test duration, the surface deterioration, expressed in (g m⁻²), is being collected, dried, and weighed. **Figure 5** shows a CDF freeze–thaw chamber, filled with containment boxes. Each containment box holds one CDF specimen. For further information regarding the standard CDF test, please refer to ref. [14].

4. 3D Scan Data

4.1. Overview

Parallel to the CDF test, the mortar samples are scanned after 0, 4, 10, 14, 18, 24, and 28 FTC. **Figure 6** shows an exemplary setup for the process of sample scanning. The freeze–thaw-exposed

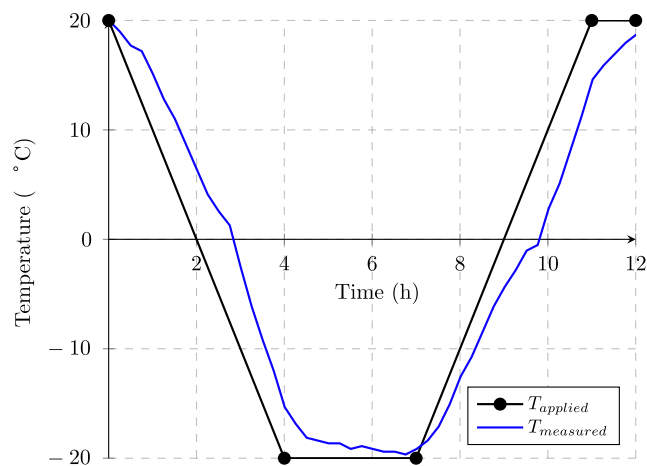


Figure 4. Visualization of the applied temperature T_{applied} and measured temperature T_{measured} of one FTC.

testing surface and the back side of the sample are both scanned with the 3D scanner (see **Figure 6a**). Prior to scanning, the sample is positioned on top of a 3D-printed mounting bracket, which is equipped with target markers. These markers are required by the scanner for orientation and generation of the coordinate system of the point cloud (see **Figure 6b**).

The following sections describe the processes of the novel methodology in detail.

4.2. Scan Data Alignment Process

The data obtained from the 3D scanner is a point cloud, i.e., list of coordinates specified in 3D space with the corresponding normals. The normal vector is used to obtain an orientation of the surface that comprises the neighborhood of a certain point. In our case, for a given specimen, we have a series of point-clouds corresponding to the state of the exposition surface after being subjected to a certain number of FTCs. In order to evaluate the relative changes to the specimen, we have to compare the scans. Given the point-cloud data of two scans corresponding to two different states of surface deterioration, the point-cloud data can be compared only if the reference coordinate system is the same in both cases. However this is not the case. Manually ensuring that the origin of the coordinate system is aligned for all subsequent scans corresponding to the level of surface deterioration is cumbersome and not accurate. Thus, we have used a computational technique to align the scans.

The strategy to automatically align scans pertaining to a certain specimen at various levels of surface deterioration is as follows. First, it is assumed that there is a surface region in the scan that is not affected by surface deterioration and whose surface characteristics such as pores and other geometrical artifacts remain constant throughout the freeze–thaw loading process. Typically, this can be the surface that is not in contact with the NaCl solution (back side of the specimens). A representative planar section of this surface is first extracted from all the scans that correspond to the same specimen. Subsequently, a transformation matrix that aligns this surface is computed using a point-set registration algorithm. This transformation matrix is then applied to the complete point cloud to obtain the final alignment. While the point-set registration procedure is a major component of the algorithm, additional preprocessing and postprocessing algorithms are required for the alignment due to the noise and the missing correspondences between the pairs of point clouds that have to be aligned.

Each alignment procedure involves two point clouds: a source and a target. The source point cloud is the point cloud corresponding to the initial state of the surface of the specimen even before being subjected to freezing and thawing loads. The reference surface state before FTC exposition of the source point cloud is first extracted using the RANdom SAmple Consensus (RANSAC) algorithm for plane detection. Given the equation of the plane corresponding to this surface, a transformation matrix that aligns this surface to the coordinate axis is extracted using translation and rotation procedures. **Figure 7** illustrates the concept of the individual steps of the determination of the transformation matrix.

It must be emphasized that at this point, the point clouds are not aligned but only the transformation matrix that aligns the

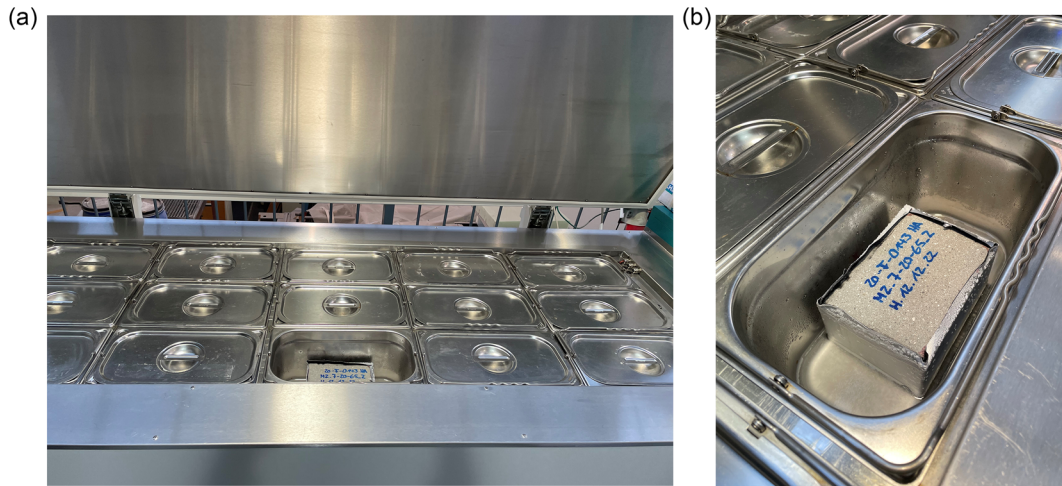


Figure 5. CDF test setup: a) containment boxes placed inside the freeze–thaw chamber; b) specimen standing in sodium chloride solution.

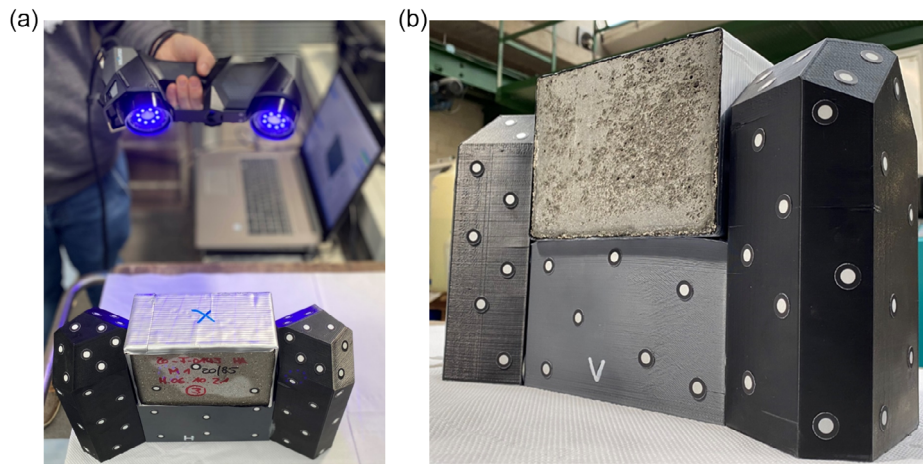


Figure 6. 3D scanning setup: a) scanning procedure showing the 3D hand-held device scanning the mortar specimen; b) specimen placed in the mounting bracket covered in white target markers.

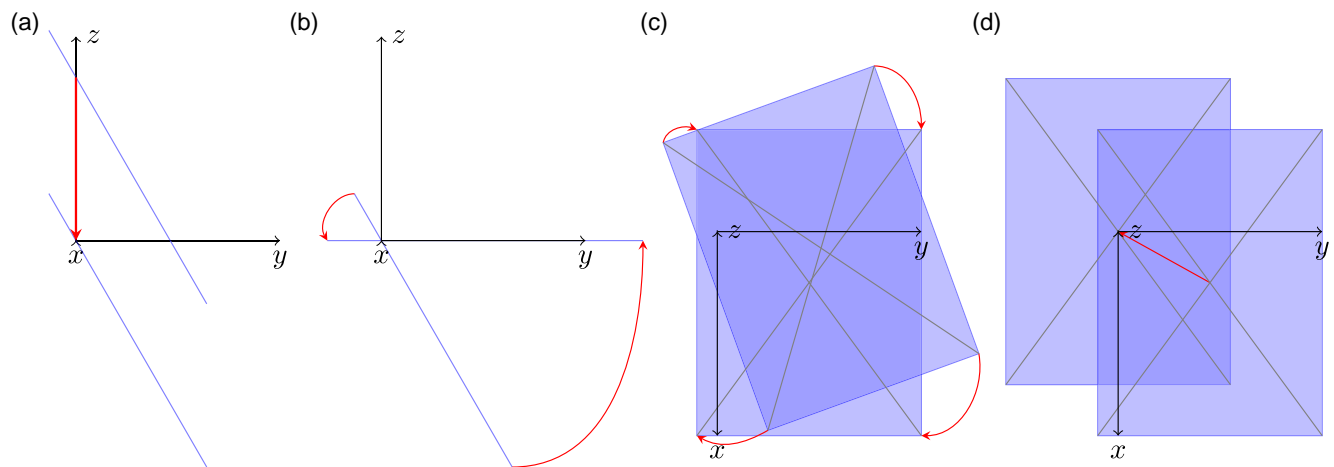


Figure 7. Subprocesses of determining the transformation matrix: a) translation of the plane to the x – y plane, b) rotation onto the x – y plane, c) alignment with the x – y axes, and d) translation to the coordinate center.

reference surface to the coordinate axis is computed. Now, the target point cloud is aligned to the source point cloud by first removing the exposition surface from the scan by simply deleting the points below a certain z-coordinate value. These two partial scans are now aligned by first applying the global fast registration algorithm^[21] followed by a local iterative closest point algorithm.^[22] After local alignment, the transformation matrix is applied to both the source and target scans. A flowchart describing this procedure is shown in **Figure 8**. Depending on the type of input file (source or target), the algorithm either generates the transformation matrix or starts the alignment process.

4.3. Data Evaluation

The aligned scan data are subsequently cropped from the original sample surface size of $\approx 150 \times 110 \text{ mm}^2$ to a predefined format of $130 \times 90 \text{ mm}^2$. This reduces each side by 10 mm to remove the sample areas potentially exposed to a 2D freeze–thaw attack. To ensure comparability between the temporal changes of the same sample as well as different concrete mixture series, the 3D coordinate nodes of the cropped sample data are aligned to the x–y coordinate grid with a linear nearest-neighbor approximation. This results in a uniform x–y orientation of every sample where only the z-axis coordinate varies. **Figure 9** illustrates the original, unaligned scan data (blue nodes) in the x–y plane (a) and the aligned mesh after approximation (b).

The z-axis component of each node is mainly used for the subsequent data analysis processes.

4.3.1. Sample Volume and Area

In addition, the x–y–z grid also allows the calculation of the sample volume and area. The volume is calculated by constructing two truncated triangular prisms for each grid segment (see **Figure 10**).

The volume of each prism is calculated according to Equation (1)

$$V_k = \frac{1}{3} A_k (h_1 + h_2 + h_{3,k}), \forall k \in \{1, 2\} \quad (1)$$

where $V_k \text{ (mm}^3\text{)}$ is the volume of the truncated triangular prism, $A_k \text{ (mm}^2\text{)}$ is the base triangle area at $z = 0$, and h_1, h_2 , and h_3 (mm) are the heights of the prism corners.

Analogously, the sample surface area is calculated by adding up the two triangle areas of each grid segment. Each triangle area is calculated with three given side lengths according to the Heron's formula (see Equation (2))

$$A_k = \sqrt{s(s - a_k)(s - b_k)(s - c)}, \forall k \in \{1, 2\} \quad (2)$$

where $A_k \text{ (mm}^2\text{)}$ is the triangle area, $s \text{ (mm)}$ is the semi perimeter, $s = \frac{a+b+c}{2}$ and $a_k, b_k \text{ (mm)}$ are the triangle side lengths (mesh size), and $c \text{ (mm)}$ is the hypotenuse length of right mesh triangle.

4.3.2. Normalized Change in Roughness

The surface area data are used to calculate the normalized change in roughness $s_{r,i} (-)$ of the surface after i FTC (see Equation (3))

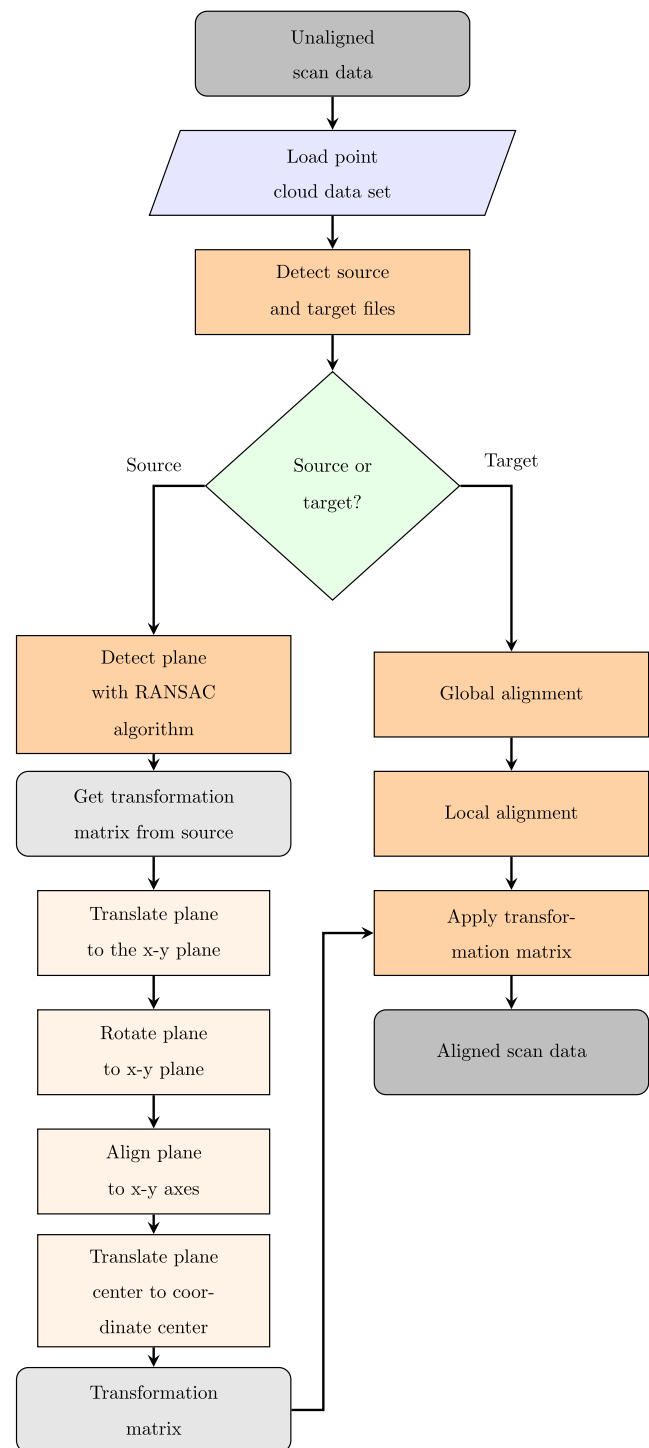


Figure 8. Flowchart of the alignment algorithm.

$$s_{r,i} = \frac{A_i^{\text{total}} - A_0^{\text{total}}}{A_0^{\text{total}}} \quad (3)$$

where $A_i^{\text{total}} \text{ (mm}^2\text{)}$ is the total surface area after i FTC and $A_0^{\text{total}} \text{ (mm}^2\text{)}$ is the total surface area at 0 FTC.

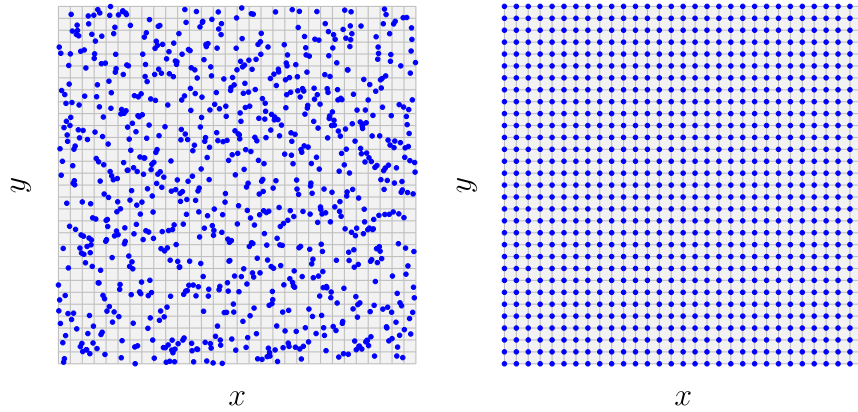


Figure 9. Concept of a) unaligned scan data nodes and b) x–y axis aligned mesh.

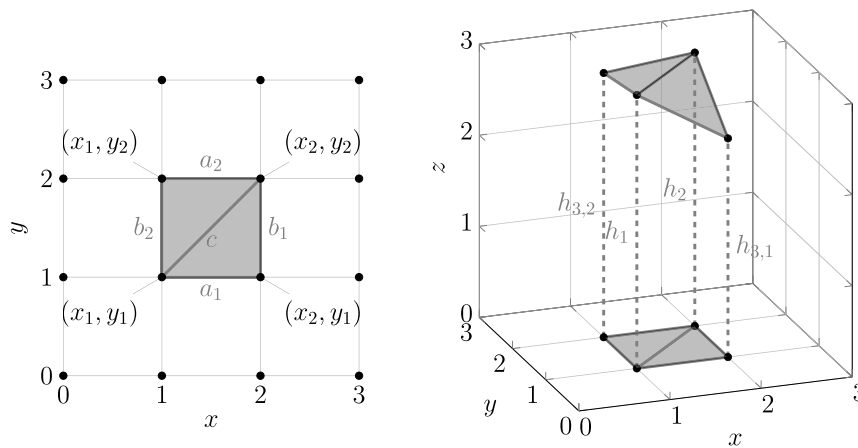


Figure 10. Concept of a) generating two truncated triangular prisms for each grid segment and b) illustrating a 3D prism with varying z-axis coordinates.

4.4. Comparison with CDF Results

In order to compare the scan data results with the CDF results, the volume results are used to determine the mass loss of the samples. For this purpose, the volume difference of the current FTC and the volume before frost exposition is being divided by the density of the sample. The mass difference is then divided by the predefined scan surface area of $130 \times 90 \text{ mm}^2$. This ultimately results in the surface deterioration w_i in g m^{-2} , analogously to the CDF surface deterioration results.

$$\Delta V_i^{\text{total}} = V_0^{\text{total}} - V_i^{\text{total}} \quad (4)$$

$$\Delta m_i = \Delta V_i^{\text{total}} \rho_i \quad (5)$$

$$w_i = \left(\frac{\Delta m_i}{A_{\text{scan}}} \right) \times 10^6 \quad (6)$$

where $\Delta V_i^{\text{total}}$ (mm^3) is the volume difference, V_0^{total} (mm^3) is the volume of the sample at 0 FTC, V_i^{total} (mm^3) is the volume of the sample after i FTC, Δm_i (g) is the mass difference, ρ_i (g mm^{-3}) is the density of the observed sample, and w_i (g m^{-2}) is the surface deterioration from scan data after i FTC. A_{scan} is the predefined

scan data area of $130 \times 90 \text{ mm}^2$ and V_0^{total} is the total volume of the sample at 0 FTC.

5. Results and Discussion

The results presented in this article are based on the testing sets shown in Table 1. After the alignment and grid approximation processes, the resulting x–y axis aligned cropped scan data act as the starting point for the data analysis.

Figure 11 shows the progress of the surface deterioration profile during the CDF test after certain FTCs of sample set M1 20-65.

Both volume and surface area of each FTC scan are compared to the values of the reference scan. This results in the volume loss and change in roughness graphs (see **Figure 12**). For samples with a high amount of surface deterioration, the change in roughness of the sample set indicates an asymptotic curve approaching a specific maximum value (maximum roughness of the surface).

Both scan data and CDF surface deterioration of sample sets M1 20–65, M1 WS, and M2 20–65 are shown in **Figure 13**. It can be observed that both methodologies for the determination of the surface deterioration deliver comparable results (M1 20–65 and

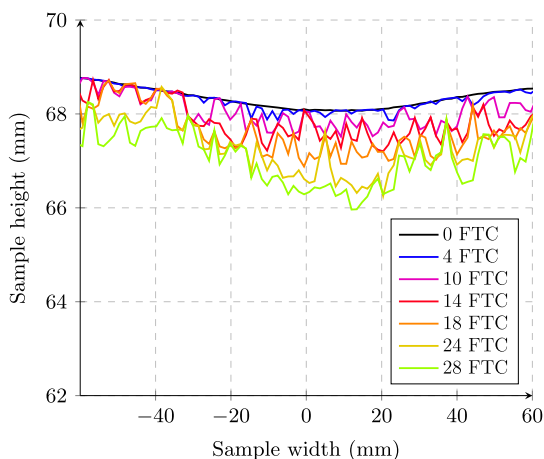


Figure 11. Variation of specimen cross section of sample set M1 20-65 as a function of FTC.

M2 20-65). For sample set M2-WS, where the surface damage is much higher compared to the aforementioned sample sets, the scan data surface deterioration delivers lower results (6000 g m^{-2}) compared to the CDF surface deterioration (9000 g m^{-2}).

Finally, **Figure 14** shows the correlation between the surface deterioration results from both the standard CDF test and the scan data of all three sample sets. Sample sets M1 20-65 and M2 20-65 deliver a good correlation with R^2 scores of 0.98 and 0.94. In contrast, testing set M1 WS results in a weaker

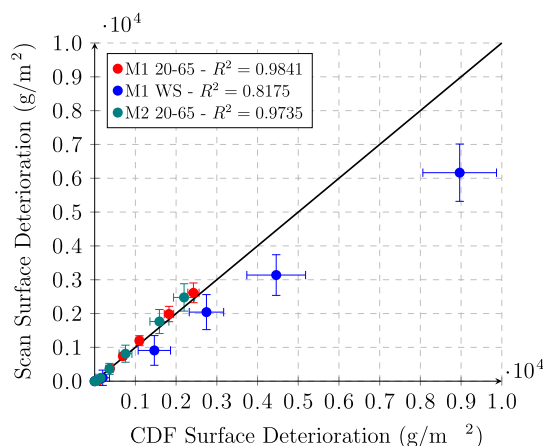


Figure 14. Correlation between surface deterioration results from CDF and scan data in (g m^{-2}).

correlation with an R^2 score of 0.82. The increased measured surface deterioration from the CDF test is caused by an additional surface deterioration effect on the vertical sides of the specimens due to isolation tape scaling. An integral premise of the CDF method is the 1D transport of moisture, which is ensured by the isolation tape on the vertical sides of the specimens. After each FTC, the scaled particles are weighed and referred to the area of the horizontal plane, which was exposed to the NaCl solution. In case of detachment of the isolation tape, additional scaling on the vertical sides of the specimens can occur. This

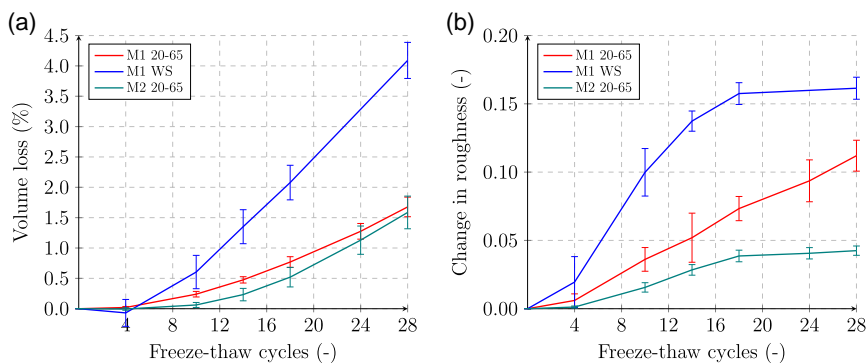


Figure 12. a) Volume loss and b) normalized change in roughness of sample sets M1 20-65, M1 WS, and M2 20-65.

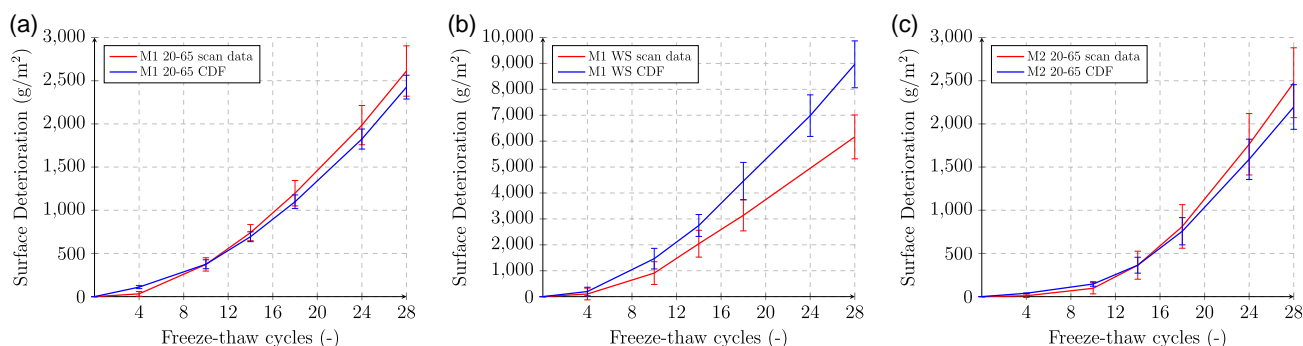


Figure 13. Scan data and CDF surface deterioration results of sample sets a) M1 20-65 in (g m^{-2}), b) M1 WS in (g m^{-2}), and c) M2 20-65 in (g m^{-2}).

additional scaling cannot be separated from the scaling of the horizontal plane during the CDF evaluation. Hence, the scaling results deliver an increased amount of surface deterioration. In the CDF method, we are measuring the material that has detached from the specimens. In the scan method, we are measuring the specimens after the detachment of the scaling particles. Hence, with the scan method, we can localize the scaling to specific regions. However, this is impossible using the traditional CDF method. According to the presented results, using the CDF method can provide an assessment of the material that suggests a weaker freeze–thaw resistance. Measuring freeze–thaw resistance is essential to buildings in cold climates. With the increased amount of weathering in the CDF evaluation, we get distorted results due to tape scaling. Hence, we get an incorrect assessment of freeze–thaw resistance of the material using the CDF method. The scan method, which can localize the scaling to specific regions of the specimens, provides a correct assessment of freeze–thaw resistance.

6. Conclusion

The methodology presented in this article delivers new information regarding the surface deterioration of the CDF test samples (depth of deterioration and change in roughness). The change of volume and area can be used to support the evaluation of the standard CDF methodology. Especially for sample sets with high amounts of surface deterioration, it is suggested to consider the surface deterioration results derived from the scan data. The performance against freeze–thaw attacks combined with deicing salt agents is assessed with the CDF test. In case of adhesive detachment of the isolation tape on the vertical sides of the specimens, additional scaling on the vertical sides of the specimens can occur. This falsifies the scaling results and overestimates the final scaling values. The presented scan method enables a localization of the scaling to specific regions of the specimens. Hence, the underestimation of the material's performance due to additional surface deterioration effects after tape scaling can be prevented using the 3D scanning methodology. Further investigations will be carried out regarding the presented 3D scan data characterization's use case and application for the evaluation of field experiment data. Also, additional data evaluation will be applied to analyze the average depth of the surface deterioration and the associated distribution function.

Acknowledgements

The authors would like to thank the German Research Foundation (DFG) for the financial support of this work within the project “Effect of intermittent drying periods on the damage development of concrete during freeze–thaw and de-icing salt attacks” (project number 428338963).

Open Access funding enabled and organized by Projekt DEAL.

Conflict of Interest

The authors declare no conflict of interest.

Data Availability Statement

The data that support the findings of this study are available from the corresponding author upon reasonable request.

Keywords

concrete, durability, freeze–thaw resistance, mortar, 3D scan

Received: February 24, 2023

Revised: May 25, 2023

Published online: July 20, 2023

- [1] United Nations, Department of Economic and Social Affairs, Population Division, (*ST/ESA/SER.A/420*), United Nations, New York, NY **2019**.
- [2] J. Stark, B. Wicht, in *Frost- Und Frost-Tausalz-Widerstand Von Beton*, Springer Berlin Heidelberg, Berlin, Heidelberg **2013**, pp. 399–471.
- [3] S. Palecki, in *Hochleistungs-beton Unter Frost-Tau-Wechselbelastung- Schädigung- Und Transportmechanismen*, Cuvillier Verlag, Göttingen, Germany **2005**.
- [4] T. C. Powers, L. E. Copeland, H. M. Mann, Capillary Continuity or Discontinuity in Cement Pastes, Technical Report, **1959**.
- [5] DIN EN 197-1:2011-11, *Cement - Part 1: Composition, Specifications and Conformity Criteria for Common Cements; German Version EN 197-1:2011*, Beuth Verlag, Berlin **2011**.
- [6] M. J. Setzer, *J. Colloid Interface Sci.* **2001**, *243*, 193.
- [7] T. C. Powers, R. A. Helmuth, in *Highway Research Board Proc.*, Vol. 32, Highway Research Board **1953**.
- [8] O. Coussy, P. J. M. Monteiro, *Cem. Concr. Res.* **2008**, *38*, 40.
- [9] G. W. Scherer, J. J. Valenza, *Mater. Sci. Concr.* **2005**, *7*, 209.
- [10] G. W. Scherer, *J. Non-Cryst. Solids* **1993**, *155*, 1.
- [11] T. Zhou, M. Mirzadeh, R. J.-M. Pellenq, M. Z. Bazant, *Phys. Rev. Fluids* **2020**, *5*, 124201.
- [12] J. J. Timothy, A. Haynack, T. Kränkel, C. Gehlen, *Appl. Mech.* **2022**, *3*, 1288.
- [13] DIN CEN/TS 12390-9:2017-05, *Testing Hardened Concrete - Part 9: Freeze-Thaw Resistance With De-Icing Salts - Scaling; German Version CEN/TS 12390-9:2016*, Beuth Verlag, Berlin **2017**.
- [14] Bundesanstalt für Wasserbau, BAW-Merkblatt Frostprüfung von Beton (MFB), **2012**.
- [15] S. Kohtala, J. F. Erichsen, O. P. Wullum, M. Steinert, *Proc. CIRP* **2021**, *100*, 762.
- [16] A. Haleem, P. Gupta, S. Bahl, M. Javid, L. Kumar, *Mater. Today: Proc.* **2021**, *39*, 331.
- [17] R. H. Helle, H. G. Lemu, *Mater. Today: Proc.* **2021**, *45*, 5255.
- [18] B. V. Farahani, F. Barros, M. A. Popescu, P. J. Sousa, P. J. Tavares, P. Moreira, *Procedia Struct. Integr.* **2019**, *17*, 712.
- [19] F. Weise, B. Maier, K. Ehrig, *Beton-und Stahlbetonbau* **2012**, *107*, 816.
- [20] Creaform, HandySCAN 3D | BLACK Series, **2022**, <https://www.creaform3d.com/en/portable-3d-scanner-handyscan-3d/technical-specifications> (accessed: July 2023).
- [21] Q.-Y. Zhou, J. Park, V. Koltun, in *European Conf. on Computer Vision*, Springer, New York **2016**, pp. 766–782.
- [22] S. Rusinkiewicz, M. Levoy, in *Proc. Third Inter. Conf. on 3-D Digital Imaging and Modeling*, IEEE, Piscataway, NJ **2001**, pp. 145–152.